

Muon Tomography sites for Colombia volcanoes

H. Asorey

*Laboratorio Detección de Partículas y Radiación,
Instituto Balseiro y Centro Atómico Bariloche,
Comisión Nacional de Energía Atómica,*

*Av. E. Bustillo 9500, (8400) San Carlos de Bariloche, Argentina;
Sede Andina, Universidad Nacional de Río Negro,
Mitre 630, (8400) San Carlos de Bariloche, Argentina y
Instituto de Tecnologías en Detección y Astropartículas*

Av. Gral. Paz 1499, (1650) San Martín, Buenos Aires, Argentina.

L. A. Núñez

*Escuela de Física, Universidad Industrial de Santander
Carrera 27 y Calle 9, 640002 Bucaramanga, Colombia y
Centro de Física Fundamental, Departamento de Física,
Universidad de Los Andes, 5101 Mérida, Venezuela.*

J.D. Sanabria-Gómez

*Escuela de Física, Universidad Industrial de Santander
Carrera 27 y Calle 9, 640002 Bucaramanga, Colombia.*

C. Sarmiento-Cano

Instituto de Tecnologías en Detección y Astropartículas

Av. Gral. Paz 1499, (1650) San Martín, Buenos Aires, Argentina.

D. Sierra-Porta

*Escuela de Física, Universidad Industrial de Santander
Carrera 27 y Calle 9, 640002 Bucaramanga, Colombia y
Centro de Modelado Científico. Facultad Experimental de Ciencias
Universidad del Zulia, 4001 Maracaibo, Venezuela.*

M. Suárez-Durán, M. Valencia-Otero and A. Vesga-Ramírez

*Escuela de Física, Universidad Industrial de Santander
Carrera 27 y Calle 9, 640002 Bucaramanga, Colombia.*

for the MuTe Collaboration

May 30, 2017

Abstract

Using a very detailed simulation chain to calculate the cosmic ray background flux, we propose most convenient places and estimate the exposure time of a muon telescope to study active Colombia volcanoes. We design and implement a simple criterion to study a dozen of active Colombia volcanoes and determined which is workable. Our simulation chain considers three important factors with different spatial and time scales: the geomagnetic effects, the development of the extensive air showers in the atmosphere, and the detector response at ground level. Considering each particular volcano topography, we obtained the muon flux crossing each structure and estimate the time exposure for our hybrid muon telescope at several point around each geological edifice, assuming a reasonable statistics for different instrument acceptances.

1 Introduction

1.1 Volcanoes in Colombia

Colombia, located in the Pacific Belt, has more than a dozen of active volcanoes (see figure 1) which can be clustered in three main groups along Cordillera Central, the highest of the three branches of the Colombian Andes.

Most of these volcanoes represent significant risk to the nearby population in towns and/or cities [1–3] and have caused major disasters with one of the most recent landmarks in the Armero tragedy (November 13, 1985), when pyroclastics of the Nevado del Ruiz fused about 10% of the mountain glacier, sending lahars with the terrible devastating result of 20,000 casualties [4].

Therefore, determining and modelling volcano inner structure is crucial to evaluate their potential risk. This might be achieved throughout powerful techniques such as muon tomography, which measures the cosmic muon flux attenuation by rock volumes of different densities, allowing the projection of images of volcanic conduits at the top of the volcanic edifice. It constitutes an engaging way to infer density distributions inside different geological structures, which is critical to study possible eruption dynamics associated to specific eruptive styles.

In this work we have considered 13 Colombian active volcanoes: Azufral, Cerro Negro, Chiles, Cumbal, Doña Juana, Galeras, Machín, Nevado del Huila, Nevado del Ruiz, Nevado Santa Isabel, Nevado del Tolima, Puracé, and Sotará. Because of their social significance and eruptive history, we shall briefly describe some of the characteristics of four of them: Galeras, Nevado del Ruiz, Cerro Machín and Cerro Negro-Chiles complex.

1.1.1 Galeras

Galeras volcanic complex, GVC, –located in the southwest Colombia: $1^{\circ}13'18.58''\text{N}$, $77^{\circ}21'33.86''\text{W}$ – is the most active volcano in Colombia with the highest social risk due to its frequent activity and the populated area.

Surpassing 5,000 years of antiquity, the GVC has a base diameter of 20 km, a summit elevation of 4,276 m a.s.l., and a main crater diameter of 320 m. The active cone, called Galeras Volcano, rises 1600 m above and approximately 9 km away from the city of San Juan de Pasto (capital of Nariño department) with a population of 313,000 inhabitants.

Galeras is characterized by andesite lava & pyroclastic with significant fallout deposits, displaying a conical shape with a big caldera at the top. After a long period of inactivity of more than 40 years, it started again in 1987, experimenting mainly minor eruptions, some with explosive

character: fumarolic formation and enlargement, strong tremors, shockwaves and emission of pyroclasts and ashes [5,6]. Since 2009, the activity has been considerably reduced to expulsion of ashes –columns that have reached 10 km– and shockwaves [7].

1.1.2 Cerro Negro - Chiles

The Chiles and Cerro Negro are located on the Colombia-Ecuador border, 86 km from the city of San Juan de Pasto, at geographic coordinates $0^{\circ}49'N$ $77^{\circ}56'W$ and $0^{\circ}46'N$ $77^{\circ}57'W$, respectively.

This volcanic complex is built at intersections of three faults: Chiles-Cerro Negro, Chiles-Cumbal and Cerro Negro-Nasta. The volcanic domes reach 4748 m a.s.l (Chiles), 4470 m a.s.l (Cerro Negro), and their craters have diameters of 1.0 km and 1.8 km, respectively. These two adjacent volcanic cones are collapsed towards the north (Chiles) and west (Cerro Negro), with presence of geoforms of already extinct glacier action. Their buildings are formed mainly by several episodes of lava and pyroclastic, with main volcanic products classified as andesites of two pyroxenes and olivines.

Although there are no historical records of eruptive activity, there is evidence of highly explosive stages and the current activity is displayed by the presence of hot springs and solfataras. On the Ecuadorian side of Chiles there is a seismological station which detect frequent activity.

1.1.3 Nevado del Ruíz

The Nevado del Ruíz volcano (NRV) is an ice-covered located at the Cordillera Central $-4^{\circ}53'43''N$ and $75^{\circ}19'21''W$ – with an altitude of approximately 5390 m a.s.l. and covering an area of more than 200 square kilometers. Its main crater (Arenas) is one kilometer in diameter and 240 m deep. La Piraña and La Olleta are two small parasitic edifices, and four U-shaped amphitheaters produced by flank collapse and fault activity [8].

It is structurally located at the junction of two fault systems: the $N75^{\circ}W$ normal Villa María-Termiales fault system and the $N20^{\circ}E$ right-lateral strike-slip Palestina fault system [9]. Its north and northwest borders show uneven geometries caused by the location of large amphitheaters on the upper part of the volcano, the southern and southwestern sides are marked by strong regular slopes while east and southeastern fringe present moderate-to-strong declivities and a significant thickness of glacial deposits.

The eruptive history of the VNR runs from the Pleistocene to the present and its stratigraphy has three main stages related to the alternate construction-destruction of its edifice: Ancestral Ruiz (2-1 megayears), Older Ruiz (0.8-0.2 megayears) and Present Ruiz (>0.15 megayears) [10]. The present emplacement of lava domes are made of andesite an dacite inside older calderas [11]. During the past 11,000 years, NRV passed through at least 12 eruption stages, which included multiple slope failures (rock avalanches), pyroclastic and lahars, leading to partial destruction of the summit domes [10,11]. The last thousand years eruptions have mostly been small, excluding some like the phreatic-magmatic eruption on November 13, 1985, which involved the partial melting of the glacier cap and consequent lahars, which reached and destroyed the municipality of Armero-Tolima and caused a large number of casualties.

1.1.4 Machín

The Machín volcano is often overlooked as a minor edifice in the Cerro Bravo-Cerro Machín volcanic belt but, considering its high explosive potential, dacitic composition and magnitude of past eruptions, it should be considered one of the most threatening active volcanoes in Colombia [12].

Also located at the Cordillera Central ($4^{\circ}29'N$ $75^{\circ}22'W$), it is situated between Cajamarca and Machín [13].

Over the last 5,000 years, Machín have had six eruptions –last one occurred about 850 years ago– generating pyroclastic, depositing several tens of centimeter ash layers, throwing eruptive columns (several tens of kilometers) and flows of volcanic mud. During present times some of the manifestations of Machín volcanic activity are: the presence of fumaroles, permanent microseismicity, thermal waters flowing in the vicinity of the crater, geoforms of the well-preserved volcanic building and greater presence of Radon gas in the sector [12].

According to studies related to the geological history of this volcano, future eruptive episode pyroclastic which would be deposited mainly in an area of 10 km^2 around the volcano edifice [14]. However, with its average height of 2750 m a.s.l; a crater of 2.4 km of diameter occupied by several domes and fumarolic activity, cause this volcano to be blended into the landscape of its nearby topography and make it practically invisible, because it does not correspond with the common image we have of a volcano. This fact increases the risk of Machín volcano for those populations that have established in its surroundings.

1.2 Muon tomography

The interest of muon tomography for Earth sciences purposes arose after the discovery of the significant penetration power of some high energy secondary particles produced by the interaction of cosmic rays with the atmosphere (hereinafter, primaries). These particles are able to cross hundreds of meters of rock with an attenuation related to the amount of matter traversed along its trajectory [15]. This type of tomography uses the same basic principles than a standard medical radiography: it measures, with a sensitive device, the attenuation of cosmic muons when crossing geological structures. Although there are limitations to muography to detect deep structures beneath the volcano (such as a magma chamber), it is particularly useful when it is applied to shallow volcano phenomena as the conduit dynamics. Thus, volcano muography constitutes an unique method to obtain direct information on the density distribution inside geological objects with a better spatial resolution than other geophysical techniques.

The directional opacity ϱ –related to the quantity of matter encountered by the muons along their path across the volcano– is obtained by comparing the muon flux Φ after crossing the target to the incident open sky flux, Φ_0 . These flux estimations are influenced by various environmental parameters –altitude, geomagnetic corrections, solar modulation and atmospheric variations– and some critical features of the instrument design. The number of detected muons is a convolution of the flux crossing the target, the exposure time and the telescope acceptance, which is the key instrumental parameter to evaluate from the simulations and/or the recorded data (see next sections).

In principle, the study of cosmic rays (and in particular the detection of these across rock) were motivated by the need to understand and describe the background noise in detectors of particles that were inside of mountainous structures, that is, several meters below the ground [16, 17] in which it is necessary not to have different signals than expected of the experiment itself. The first muon radiography was made by L. Álvarez [18] in the pyramid of Cheops. Later, the utility of muon imaging in mining geophysics were developed [19] and more interesting applications emerge when lighter and mobile detectors became available.

More recently, a new era of significant improvements in particle detectors and miniaturized electronics has renewed the interest for muon imaging applied to geological structures. Japanese

and French teams have demonstrated the feasibility to monitor spatial and temporal changes of density distributions inside volcanoes (see [20–30] and references therein). Even more, there has been a significant amount of research around this astroparticle application to the study of interior of volcanoes structures. In this context the references [23,25–28,31–35] report the general principles and particular applications of this technique.

The main objective of the present work is twofold: first, to contribute to identify possible muon telescope observation sites for Colombia active volcanoes and second, to estimate the possible detected muon flux for our hybrid muon telescope at those sites. It has been implemented formulating simple and general criteria about the feasibility to place a muon telescope in a candidate volcano which will be presented in the coming section. Next, in section 2.2, we describe the detailed simulation chain to estimate the incoming incident atmospheric muon fluxes. With this detailed flux estimation we examine, in section 2.3, the energy loss of muons crossing the volcano edifice. For completeness our hybrid muon telescope is briefly sketched in section 2.4. Next, in section 3 we discuss the results of the application of our criterion to 13 Colombia volcanoes and implement the simulation for the muon rock propagation. There, we show estimations the outgoing muon flux from the geological structures that could be detected by our telescope. Finally, in the section 4 conclusions are presented along with possible future works.

2 Methods

2.1 Volcano observation site determination criteria

It is worth mentioning that the criteria for determination of muon observation sites for mainland volcanoes, –surrounded by other geological structures that could screen the atmospheric muon flux– is qualitatively different than those made on island volcanoes, free from the screening of other mountain systems.

So, to determine muon observation points for active volcanoes in Colombia, we establish a blend of technical and logistic items, which we call the “thumb criteria” that should be fulfilled by potential sites and are listed below:

Criterion 1: At the observational level, is the volcano base width less than 1,500 m? This criterion is considered because the energy of atmospheric horizontal muons are two orders of magnitude lower than vertical muons and, these incident particles need two more orders of magnitude to cross the volcanic structure [36]. Therefore, most energetic horizontal muons can only cross 1,500m of standard rock and the horizontal line of sight from the tentative observation point should cross less than this distance.

Criterion 2: Are there tentative observation points where the surrounding topography does not affect the target? Muons impacting the telescope should cross only the direct structure under study. Nearby mountains and any other geological formations neighboring the target volcano, must not contribute to the opacity. Obviously this impose a severe restriction on the tentative observational points to a few places where only a small observational window is present, with no mountains or other geological structures behind.

Criterion 3: Are the sites accessible and secure? Site must be easily accessible and the telescope can be securely transported and placed on field. It is important to consider: the weight and size

of the assembled telescope and its parts; also the quality and accessibility of water resources in the area, because the telescope requires approximately two cubic meters of purified water.

Criterion 4: Are the sites safe? Although it is true that the response of volcanoes is as unpredictable as nature itself, one must keep in mind the risk factor of the volcano. The volcano to be studied should not be cataloged in a situation of abundant activity due to the danger of volcanic products and processes associated with eruptions such as ash fall, pyroclastic materials, lahars, floods, among other risk, as well as earthquakes and landslides that may cause serious damage to instrument and personnel.

We have implemented the first two criteria with a ray tracing code which determines all possible muon paths from 10 different tentative observational points at each volcano. Next we calculate rock distances crossed by each muon path, considering in detail the topography around each volcano which is available from NASA Shuttle Radar Topography Mission (SRTM) global digital elevation model of Earth¹, with SRTM3 resolution 90m×90m. We apply this code choosing 10 tentative observation points complying the third criterion to the above 13 mentioned volcanoes.

2.2 Muon flux simulation chain

As the particles measured at ground (secondaries from now on) are produced by the interaction of primaries with the atmosphere, the modulation of secondary particles needs to be monitored and carefully corrected by taking into account atmospheric factors that could modify the flux of secondaries at Earth surface. Thus, a complete and detailed simulation chain is needed to characterize the expected flux at the detector level, considering factors such as geomagnetic conditions, atmospheric reaction and detector response [37, 38].

Nowadays computational capabilities allows the extension of the usual approach, i.e., to consider only the main components of the GCR flux locally and include geomagnetic effects by an effective rigidity cutoff for vertical primaries. Clearly any attempt to estimate the expected flux of secondaries at any detector should be based on a detailed simulation that takes into account any possible source of flux variation. This complex approach comprises process occurring at different spatial and time scales, following this conceptual schema:

$$\begin{array}{ccccccc} \text{GCR Flux} & \rightarrow & \text{Heliosphere} & \rightarrow & \text{Modulated Flux} & \rightarrow & \text{Magnetosphere} \\ \cdots \rightarrow & & \rightarrow & & \rightarrow & & \text{Primaries} \rightarrow \cdots \\ & & \text{Atmosphere} & & \text{Secondary} & & \\ & & \rightarrow & & \rightarrow & & \text{Detector response} \\ & & & & & & \text{Signals.} \end{array}$$

Our simulation pipeline considers three important factors with different spatial and time scales: the geomagnetic effects, the development of the extensive air showers in the atmosphere, and the detector response at ground level.

The effects of the geomagnetic field (GMF) on the propagation of charged particles, contributing to the background radiation at ground level, is characterized by the directional rigidity cut-off, R_c , at the detector site. This is calculated using the MAGNETOCOSMICS code, [39] which implements the backtracking technique [40]. GMF at any point of Earth is calculated by using the International Geomagnetic Field Reference (IGRF) version 11 [41], for modeling the near-Earth GMF ($r < 5R_{\oplus}$) and the Tsyganenko Magnetic Field model version 2001 [42] to describe the outer GMF.

The second step of the chain is based on the CORSIKA code [43]. Extensive air showers produced during the interaction of the measured flux of primaries in the range $1 \leq Z \leq 26$ (proton to

¹See: <http://www2.jpl.nasa.gov/srtm/>

irons) with the atmosphere are simulated with extreme detail to obtain a very comprehensive set of secondaries at ground level. We have set CORSIKA specially tuned simulation parameters as: zenith incidence of primaries between 0° and 90° (all range); primary energy range between 5 GeV and 10^6 GeV; time of simulation 48 hours (172,800 s); for the atmosphere model the tropical parameterization is used prepared specially for each particular latitude and longitude; the horizontal and vertical magnetic field component² are $B_X = 27.18 \mu\text{T}$ and $B_Z = 14.617 \mu\text{T}$, respectively. For the hadronic model of interaction in the distribution of secondary at the level of the detector we use the model QGSJET-II-04 [44] and for low energies we choose the default option, GHEISHA-2002 [45].

Finally the detector response to the different types of secondary particles at ground level is simulated by means of a GEANT4 model [46, 47] for both the scintillators panel and the water Cherenkov detector, but this last step of the simulation chain will not be considered here but detailed in a future work [48].

2.3 Muon rock opacity

To identify possible muon observation sites in Colombia, we shall implement the previously described calculation schema only at geomagnetic secular conditions, –i.e. static geomagnetic corrections– and then focus on the detailed calculation of the crossing muon flux and on the stopping power of the volcano edifice at different Colombia volcano sites.

In this first approach, we are assuming that the trajectories of muons are straight lines which are not affected by Coulomb scattering processes, therefore, the density distribution within volcano edifices can be inferred from the variation of the muon flux crossing the geological structure. A more detailed calculation, including second order effects, is being carried and will be included in future characterization of the selected places. Obviously, this variation is related to the rock opacity for each muon trajectory.

The rock opacity corresponds to the density ρ integrated along the muon path L and it can be expressed in g cm^{-2} , as:

$$\varrho(L) = \int_L \rho(\xi) d\xi = \bar{\rho} \times L, \quad (1)$$

where ϱ is the opacity or integrated mass density, ξ is a characteristic longitudinal coordinate through volcano, L is total distance traveled by muons in the rock, $\bar{\rho}$ is average density within the volcano.

Taking into account the volcano size compared to the telescope, the muon trajectories along the structure have a conical geometry with the telescope at the vertex. The energy loss along each path can be modeled as

$$-\frac{dE}{d\varrho} = a(E) + b(E)E, \quad (2)$$

for each muon arrival direction considering a constant density distribution. Here E is the muon energy; $a(E)$ and $b(E)$ are functional parameters depending on the rock composition/properties and $\varrho(L)$ is the density integrated along the trajectory of the muons (the opacity defined by eq. (1)). The coefficient $a(E)$ represents the energy loss due to ionization, while $b(E)$ takes into account the contribution radiative losses, mainly Bremsstrahlung, nuclear interactions and pair production. The main parameters to estimate the coefficients $a(E)$ and $b(E)$ are the average ratio $\langle Z/A \rangle$ between the atomic and mass numbers of the material [49].

²Values referred by: <http://www.ngdc.noaa.gov/geomag-web>

In this work, standard rock has been assumed ($\bar{\rho} \approx 2.65 \text{ g cm}^{-3}$) to estimate of the muon flow across the volcano and the coefficients $a(E)$ and $b(E)$ are obtained from the Particle Data Group³. To simulate the volcanic chimney, we assumed a lower density of 2.38 g cm^{-3} , i.e. the density is reduced by 10% at the central part of the edifice.

2.4 MuTe: Colombia Muon Telescope

There are three types of detectors which have been used for volcano muography: (a) nuclear emulsion detectors, (b) scintillation detectors, and (c) gaseous detectors. Each one has its pros and cons as are described in [33]. We have design a new hybrid Muon Telescope (MuTe), combining the facilities of a two panel scintillators hodoscope and a water Cherenkov detector, which will be capable to estimate not only the direction but a range of energies of the detected muons.

Just for completeness and to close this section, we shall briefly describe our muon telescope and its acceptance, which is critical to determine the time exposure of the instrument. A detailed description of the instrument capabilities will be discussed shortly elsewhere [48].

2.4.1 The instrument

MuTe is a hybrid instrument, combining two detection techniques –an hodoscope formed by two detection planes of plastic scintillator bars, and a water Cherenkov detector (WCD)– in an innovative manner which differentiates it from some other previous detectors.

Scintillators panels: Inspired by the experiences of other volcano muography experiments [50, 51], we have designed two X-Y scintillating parallel arrays of $30 \times 30 = 900$ pixels of $4 \text{ cm} \times 4 \text{ cm} = 16 \text{ cm}^2$, which sums up $14,400 \text{ cm}^2$ of detection surface. The panels can be separated up to $D = 200 \text{ cm}$ (see figure 2) and are mounted on a modular frame which can be easily transported and assembled at the installation site.

Water Cherenkov Detector: The WCD is a purified water cube of 120 cm side –located behind the rear scintillator panel (see figure 2)– which acts as absorbing element and as a third active coincidence detector. Due to its dimensions and its location, our WCD filters most of the background noise (low energies electrons, protons and muons moving in reverse) which could cause overestimation in the hodoscope counts [52]. Additionally it also add an other detector, in coincidence with the hodoscope, to estimate the energy spectrum of the detected muons.

2.4.2 Telescope acceptance

The incident number of muons $N(\varrho)$ is

$$N(\varrho) = \Delta T \times \mathcal{T} \times I(\varrho), \quad (3)$$

where $I(\varrho)$ is the integrated flux (measured in $\text{cm}^{-2} \text{sr}^{-1} \text{s}^{-1}$), \mathcal{T} represents the acceptance (measured in $\text{cm}^2 \text{sr}$), ΔT designates the exposure time (in seconds), and $\varrho(L)$ the opacity parameter which is related to the muon absorption in the constituent material of the geological object [23].

The acceptance of the instrument is a convolution of the telescope geometry (number of pixels, pixel size, and panel separation) and it is obtained by multiplying the detection area with the angular resolution,

$$\mathcal{T}(r_{mn}) = S(r_{mn}) \times \delta\Omega(r_{mn}). \quad (4)$$

³Tables on: <http://pdg.lbl.gov/2011/AtomicNuclearProperties/>

where r_{mn} represent a discrete direction on the possible muon incoming direction.

The number of discrete directions in an array of two panels with $N_x \times N_y$ pixels is understood as the distinct trajectories that can be observed impacting both panels. In this sense only one discrete direction is possible in the normal direction to the panels since all this trajectories have the same angle. For the other discrete paths with distinct angles we will have $2N_x(N_y - 1) + 2N_y(N_x - 1)$ discrete directions, i.e. $(2N_x - 1)(2N_y - 1)$ different trajectories [23].

In figure 3 we show the angular resolution and the acceptance function for our telescope (with 900 pixels and 3481 discrete r_{mn} directions). As it can be seen in this figure, the total angular aperture of the telescope is roughly 582 mrad with the maximum point at 1.6×10^{-3} sr and, as expected, the largest detection surface corresponds to the normal direction r_{00} , reaching $\approx 6 \text{ cm}^2 \text{ sr}$.

Considering muons traversing 250 m of standard rock, with density of 2.65 g cm^{-3} , and assuming an average penetrating integrated flux of $10^{-5} \text{ cm}^2 \text{ sr}^{-1} \text{ s}^{-1}$ [15] and a telescope acceptance of $\approx 6 \text{ cm}^2 \text{ sr}$, we estimate to have an expected rate up to $\approx 5 \text{ muons day}^{-1}$ for each direction r_{mn} . Moreover, as explained in [23], in our telescope configuration it is possible to obtain a simple relationship between the exposure time and the desired opacity resolution. Starting from equation (3), it is possible to show that

$$\Delta T \times \mathcal{T} \times \frac{\Delta I^2(\varrho_0, \delta\varrho)}{I(\varrho_0)} > c, \quad (5)$$

where $\Delta I(\varrho_0)$ is the flux variation due to the different opacities ϱ_0 and $\varrho_0 + \delta\varrho$, and c is a parameter measuring the confidence level in terms of the standard deviation of the measurement. The above expression give a bound for the minimum exposure time needed in order to distinguish opacity differences across the geological object.

3 Results

We applied the criteria described in section 2.1 for the above 13 mentioned volcanoes, recommended by the Colombian Geological Service (SGC). Most observation points at those volcanoes present considerable challenges and difficulty to access to transport and assemble our instrument, as well as dangerous sites due to unfavorable conditions in the event of a possible volcanic eruption.

The results of the application of the above criteria to 13 Colombian Volcanoes are summarized in table 1 and it is clear that the only Colombian volcano that could possibly be studied through muography is Cerro Machín [53].

Following our presentation in section 2, we setup the pipeline of the simulation detailed in section 2.2 for the geographic coordinates of Cerro Machín (altitude 2750 m a.s.l, $4^\circ 29' \text{N}$ $75^\circ 22' \text{W}$).

In figure 4 we show the expected momentum spectrum of the open sky secondaries flux for this site. As it can be easily noticed, at high secondary energies the particle angular integrated flux is dominated by energetic muons, with the maximum at $\approx 100 \text{ muons m}^{-2} \text{ s}^{-1} (\text{GeV}/c)^{-1}$ for momentum $4 \text{ GeV}/c$. The muon flux almost vanishes for $p_\mu \simeq 10^4 \text{ GeV}/c$. Beyond this value the flux is dominated by fluctuations introduced by the flux of high energy primaries $\gtrsim 1 \text{ PeV}$ or prompt muons originated during several-TeV EAS initial development. Our analysis concludes that, starting from a few GeV/c there is no significant effect of the geomagnetic correction on the muon flux at this geographical zone, but it is however important in the determination of the particle background flux in the site.

We have identified and displayed in Table 2, four points around the Machín volcano that comply with our “thumb criteria” and are suitable to obtain significant amount of data in reasonable

Volcano	Criterion 1:	Criterion 2:	Criterion 3:	Criterion 4:
Azufral	N	Y	N	Y
Cerro Negro	Y	Y	N	Y
Chiles	Y	Y	N	Y
Cumbal	N	Y	N	Y
Dona Juana	N	Y	N	Y
Galeras	Y	N	Y	Y
Machín	Y	Y	Y	Y
Nevado del Huila	N	Y	N	Y
Nevado del Ruíz	N	Y	Y	Y
Nevado Santa Isabel	N	Y	Y	Y
Nevado del Tolima	N	N	Y	Y
Puracé	N	Y	Y	Y
Sotará	N	Y	N	Y

Table 1: Which Colombian volcano can be studied by muography? The criteria discussed in section 2.1 has been applied to 13 Colombian volcanoes. The answer for the four question that conform the criteria can be stated as: **1**: Is the volcano base less than 1,500 m?; **2**: The surrounding topography does not affect the target?; **3**: Are the sites accessible and secure?; and **4**: Are the sites safe? Our studies suggest that only Cerro Machín obtains four positive answers.

exposure times (less than six months).

Cerro Machín points	P ₁	P ₂	P ₃	P ₄
Latitude (°N)	4.492	4.491	4.493	4.494
Longitude (°W)	75.381	75.380	75.392	75.388
Distance to center of the edifice (m)	836	946	762	730
Maximum observed depth (m)	208	228	250	190

Table 2: Feasible observation points at Cerro Machín volcano ($4^{\circ}29'23.08''$ N, $75^{\circ}23'15.39''$ W) complying with the “thumb criteria” described in section 2.1. The maximum observed depth are those points where the emerging muon flux is less than 10^{-2} muons per cm^2 per day, corresponding to zenith angles $\theta \approx 82$.

Next, we calculate the differential flux of muons at each of the above points, **P**₁, **P**₂, **P**₃, **P**₄, as a function of the direction of arrival. The maximum of muon flux is found at the zenith and it vanishes at angles very close to 90° . In figure 5 we can see an output of the calculations made for the determination of the distances of propagation of the muons in rock, as well as the angular distribution of these distances along the zone that concentrates the crater of the volcano for the observation point **P**₁. The input for these calculations is the muon flux simulations previously described. In figure 6 the muon spectra depending on particle energy trajectory through the volcano is shown. As it can be clearly appreciated, the muon flux decreases considerably until $1 \text{ cm}^{-2} \text{ sr}^{-1} \text{ day}^{-1}$ for $p_\mu \simeq 500 \text{ GeV}/c$. For those trajectories, muons cross about 600 meters on rock. Using the simple model of propagation in rock described above, the flux variation ranges from 1.8×10^3 to $1.5 \times 10^6 \text{ cm}^{-2} \text{ sr}^{-1} \text{ day}^{-1}$ for bulk densities of 2.65 g cm^{-3} for standard rock. Due the scale and dimensions of the volcano, only the first 200 m of depth measured from the top of the edifice can be

analyzed with this technique. Figure 7 displays the result the simulations of four days of muon flux crossing the volcano and measured from the observation point P1, as it could be measured by our 30×30 pixels telescope with a inter-panel distance of 200 cm. Due to the low muon high energy flux, which is then propagated by the volcano and due the angular binning induced by the high number of pixels presented in our telescope, some artificial zeros are observed. Of course, those zero-flux pixels are fluctuations, which can be corrected by artificially re-sampling the muon flux or, of course, by augmenting the time of simulation. However, using the available data we observed that, for this energy range, the muon absorption in the rock follows a power-law with the dimensionless distance traveled, x , of the form transmitted muon flux $\simeq \alpha_0 x^{\beta_0}$, with $\alpha_0 = 241.9 \text{ cm}^{-2} \text{ sr}^{-1} \text{ day}^{-1}$ and the $\beta_0 = -1.59$, with a correlation coefficient of $R^2 = 0.9575$.

Comparing figures 5 and 7, we can clearly appreciate that there is a region corresponding to zenith angle $76 < \theta < 84$ and azimuth angle $116 < \phi < 130$ where the muon flux is highly absorbed due to the volcano geometry and the distances traveled by the muons within the volcano could easily exceed 900 meters of rock before they are detected.

As explained before, exposure times, opacity (directional average density) and instrument resolution are linked through equation (5) for a given telescope configuration [23]. As an example, the expected exposure times needed to resolve average density differences of -10% respect standard rock are shown in figure 8, for the zenithal range $66^\circ < \theta < 84^\circ$. Depending on the telescope configuration and the volcano geometry as seen from the selected observation point, we obtain for then point **P₁** at Cerro Machín exposure time lapses between two days up to more than six months to obtain the desired density resolution.

4 Discussion and Conclusions

In this work, we have presented some preliminary results of the application of the muography technique to inland volcanoes in Colombia. We identified the best volcano to be studied through this emerging technique; we also spotted the finest points to place a muon telescope around it and estimate the time exposures of the instrument to obtain a significant statistic of muon flux.

We base our approach to this technique on comprehensive simulation chain to calculate the background flux at the volcano site, next we compute the muon propagation through the geological edifice taking into account a precise topographical information. Finally, we estimate the exposure time for our hybrid muon telescope.

The rationale of our new approach stems from a four-step methodology:

1. **A “thumb criteria”.** We have established a blended of technical and logistic items –the “thumb criteria”– and applied them to 13 Colombia volcanoes. We have found that only Cerro Machín, located at the Cordillera Central ($4^\circ 29' \text{N}$ $75^\circ 22' \text{W}$), could be feasibly studied through muography.
2. **A unabridged simulation of open sky particle spectrum and composition.** The energy spectrum and composition of open sky secondaries at Cerro Machín have been calculated by CORSIKA and filtered with MAGNETOCOSMICS frameworks, providing a detailed description of different types of particles in the MeVs to TeVs secondary energy range [37,38].
3. **A detailed calculation of the emerging muon flux.** With the above open sky particle flux and a precise topographic information surrounding the volcano, we have simulated the

muon propagation inside the geological edifice and estimated emerging muon flux at four different points around Cerro Machín.

4. **An estimation of the telescope time exposure.** With the emerging muon flux we have calculated the time exposures of the instrument for an statistics of 1000 events and for different values of the telescope acceptance.

As we have mentioned before, most of the previous muography studied volcanoes –Mount Asama [35] in Japan; Puy de Dôme [?] in France; Mont Etna [31] in Italy; La Soufrière [24] in Guadalupe, just to mention the most significant studies– are topographically isolated with relatively accessible observation points. There are not surrounding geological structures screening the scarce high energy horizontal muons. But Colombia is very different, most of the active volcanoes are along the Cordillera Central, surrounded by higher altitudes shielding cosmic ray flux over the volcanoes. Therefore, we developed a methodology to identify possible feasible candidates and only Cerro Machín emerges as a possibility.

Instead of using phenomenological and pseudo-empirical formulas to estimate the background flux at the volcano site (see [35] and references therein), we proceed to simulate its spectrum and composition, at each particular geographical site with two standard astroparticle tools: CORSIKA and MAGNETOCOSMICS. We found that incident muons range from 0.1 GeV/c to 10 TeV, and the flux of high energy muons is very feeble: ≈ 10 muons per square meter per day at zenith angles $\theta \approx 82 - 84$.

With the above simulation as an input, and including a precise topographical information, we calculate the propagation of muon through the geological edifice and determine the emerging muon flux that could be detected at several particular observation points around the volcano. Then, to discriminate density variations of the 10%, we evaluate time exposures of our hybrid instrument as a function of the acceptance. With these preliminary results and by considering the standard configuration of our telescope, we have estimated observation time lapses from 2 days to 125 days at the upper 114 m of the volcano edifice to significatively observe differences of 10% in the averaged density.

Muography can not image deep volcano structures but it seems to be useful to determine its shallow phenomena with an excellent spatial resolution. Obviously, this technique can not give direct information on when a volcano will erupt, but it could provide significant insights about a possible upper eruption processes. This emerging technique requires significant developments concerning treatment, understanding, and interpretation of the experimental data obtained and its future depends on synergy of two strong international community: elementary particle physicists and geophysicists [33].

Acknowledgments

The authors acknowledge the financial support of Departamento Administrativo de Ciencia, Tecnología e Innovación of Colombia (ColCiencias) under contract FP44842-051-2015 and to the Programa de Cooperación Nivel II (PCB-II) MINCYT-CONICET-COLCIENCIAS 2015, under project CO/15/02. We are also very thankful to LAGO and to Pierre Auger Collaboration for its continuous support. Finally, we would like to thank Vicerrectoría Investigación y Extensión Universidad Industrial de Santander for its permanent sponsorship. DSP wants to thank the GIRG, Grupo Halley and Vicerrectoría Investigación y Extensión of Universidad Industrial de Santander for the hospitality during my post-doctoral fellowship.

References

- [1] Gloria Patricia Cortés. Informe de actividad volcánica segmento norte de colombia diciembre de 2016. Technical report, Reporte interno, Manizales, Colombia. INGEOMINAS, 2016.
- [2] A. Agudelo. Informe técnico de actividad de los volcanes nevado del huila, puracé y sotará, durante el periodo de diciembre de 2016. Technical report, Reporte Interno, Popayan, Colombia, Servicio Geológico Colombiano, 12 2016.
- [3] Edgar Muñoz. Informe mensual de actividad de los volcanes galeras,cumbal,chiles y cerro negro, las ánimas, dona juana y azufral. Technical report, Reporte interno, Pasto, Colombia. INGEOMINAS, 2017.
- [4] Thomas C Pierson, Richard J Janda, Jean-Claude Thouret, and Carlos A Borrero. Perturbation and melting of snow and ice by the 13 november 1985 eruption of nevado del ruiz, colombia, and consequent mobilization, flow and deposition of lahars. *Journal of Volcanology and Geothermal Research*, 41(1-4):17–66, 1990.
- [5] Marta Lucia Calvache, Gloria Patricia Cortés, and Stanley N Williams. Stratigraphy and chronology of the galeras volcanic complex, colombia. *Journal of Volcanology and Geothermal Research*, 77(1):5–19, 1997.
- [6] Fernando Gil Cruz and Bernard A Chouet. Long-period events, the most characteristic seismicity accompanying the emplacement and extrusion of a lava dome in galeras volcano, colombia, in 1991. *Journal of Volcanology and Geothermal Research*, 77(1):121–158, 1997.
- [7] Gloria Patricia Cortés and Jaime Raigosa. A synthesis of the recent activity of galeras volcano, colombia: Seven years of continuous surveillance, 1989–1995. *Journal of volcanology and geothermal research*, 77(1):101–114, 1997.
- [8] S K Sennert. Global volcanism program 2016. Technical Report 10, Smithsonian Institution and US Geological Survey, 2016. Report on Nevado del Ruiz (Colombia), Weekly Volcanic Activity Report.
- [9] C Borrero, LM Toro, M Alvarán, and H Castillo. Geochemistry and tectonic controls of the effusive activity related with the ancestral nevado del ruiz volcano, colombia. *Geofísica internacional*, 48(1):149–169, 2009.
- [10] J-C Thouret, JM Cantagrel, R Salinas, and A Murcia. Quaternary eruptive history of nevado del ruiz (colombia). *Journal of Volcanology and Geothermal Research*, 41(1-4):225–251, 1990.
- [11] Christian Huggel, Jorge Luis Ceballos, Bernardo Pulgarín, Jair Ramírez, and Jean-Claude Thouret. Review and reassessment of hazards owing to volcano–glacier interactions in colombia. *Annals of Glaciology*, 45(1):128–136, 2007.
- [12] Gloria Patricia Cortés. Estudio geológico de los depósitos de lahar asociados a la actividad eruptiva del volcán cerro machín. Technical report, Reporte interno, Manizales, Colombia. INGEOMINAS, 2001.

- [13] H Cepeda, LA Murcia, ML Monsalve, RA Méndez, and A Núñez. Volcán cerro machín, departamento del tolima, colombia: Pasado, presente y futuro. Technical report, INGEOMINAS, Informe interno, 1995.
- [14] HF Murcia, MF Sheridan, JL Macías, and GP Cortés. Titan2d simulations of pyroclastic flows at cerro machín volcano, colombia: Hazard implications. *Journal of South American Earth Sciences*, 29(2):161–170, 2010.
- [15] K. Nagamine. *Introductory muon science*. Cambridge University Press, 2003.
- [16] E.P. George. Cosmic rays measure overburden of tunnel. *Commonwealth Engineer*, 1:455–457, 1955.
- [17] A. Zichichi, O. Barnabei, P. Pupillo, and F.R. Monaco. *Subnuclear Physics: The First 50 Years: Highlights from Erice to ELN*, volume 24. World scientific, 2000.
- [18] L.W. Alvarez, J.A. Anderson, F. El Bedwei, M. Sharkawi, and L. Yazolino. Search for Hidden Chambers in the Pyramids. *Science*, 167(3919):832–839, February 1970.
- [19] L. Malmqvist, G. Jönsson, K. Kristiansson, and L. Jacobsson. Theoretical studies of in-situ rock density determinations using underground cosmic-ray muon intensity measurements with application in mining geophysics. *Geophysics*, 44(9):1549–1569, 1979.
- [20] HKM Tanaka, K Nagamine, SN Nakamura, and K Ishida. Radiographic measurements of the internal structure of mt. west iwate with near-horizontal cosmic-ray muons and future developments. *Nuclear Instruments and Methods in Physics Research Section A: Accelerators, Spectrometers, Detectors and Associated Equipment*, 555(1):164–172, 2005.
- [21] H.K.M. Tanaka, T. Uchida, M. Tanaka, H. Shinohara, and H. Taira. Cosmic-ray muon imaging of magma in a conduit: Degassing process of satsuma-iwojima volcano, japan. *Geophysical Research Letters*, 36(1), 2009.
- [22] H.K.M. Tanaka, T. Kusagaya, and H. Shinohara. Radiographic visualization of magma dynamics in an erupting volcano. *Nature communications*, 5, 2014.
- [23] N Lesparre, D Gibert, J Marteau, Y Déclais, D Carbone, and E Galichet. Geophysical muon imaging: feasibility and limits. *Geophysical Journal International*, 183(3):1348–1361, 2010.
- [24] N. Lesparre, D. Gibert, J. Marteau, J.C. Komorowski, F. Nicollin, and O. Coutant. Density muon radiography of la soufrière of guadeloupe volcano: comparison with geological, electrical resistivity and gravity data. *Geophysical Journal International*, 190(2):1008–1019, 2012.
- [25] J. Marteau, D. Gibert, N. Lesparre, F. Nicollin, P. Noli, and F. Giacoppo. Muons tomography applied to geosciences and volcanology. *Nuclear Instruments and Methods in Physics Research Section A: Accelerators, Spectrometers, Detectors and Associated Equipment*, 695:23–28, 2012.
- [26] C Cârloganu, V Niess, S Béné, E Busato, P Dupieux, F Fehr, P Gay, D Miällier, B Vulpeşcu, P Boivin, C Combaret, P Labazuy, I Lakhtineh, J F Lénat, L Mirabito, and A Portal. Towards a muon radiography of the Puy de Dôme. *Geoscientific Instrumentation, Methods and Data Systems*, 2(1):55–60, 2013.

- [27] A Portal, P Labazuy, J-F Lénat, S Béné, Pierre Boivin, E Busato, C Cârloganu, C Combaret, P Dupieux, F Fehr, et al. Inner structure of the puy de dome volcano: cross-comparison of geophysical models (ert, gravimetry, muon imaging). *Geoscientific Instrumentation Methods and Data Systems*, 2:47–54, 2013.
- [28] H.K.M. Tanaka. Subsurface density mapping of the earth with cosmic ray muons. *Nuclear Physics B-Proceedings Supplements*, 243:239–248, 2013.
- [29] H.K.M. Tanaka. Particle Geophysics. *Annual Review of Earth and Planetary Sciences*, 42(1):535–549, May 2014.
- [30] R. Nishiyama, Y. Tanaka, S. Okubo, H. Oshima, H.K.M. Tanaka, and T. Maekawa. Integrated processing of muon radiography and gravity anomaly data toward the realization of high-resolution 3-d density structural analysis of volcanoes: Case study of showa-shinzan lava dome, usu, japan. *Journal of Geophysical Research: Solid Earth*, 2014.
- [31] D. Carbone, D. Gibert, J. Marteau, M. Diament, L. Zuccarello, and E. Galichet. An experiment of muon radiography at mt etna (italy). *Geophysical Journal International*, 196(2):633–643, 2014.
- [32] K Jourde, D Gibert, J Marteau, J Bremond d’Ars, S Gardien, C Girerd, J-C Ianigro, and D Carbone. Experimental detection of upward going cosmic particles and consequences for correction of density radiography of volcanoes. *Geophysical Research Letters*, 40(24):6334–6339, 2013.
- [33] H. K. M. Tanaka. Visualization of the internal structure of volcanoes with cosmic-ray muons. *Journal of the Physical Society of Japan*, 85(9):091016, 2016.
- [34] S Okubo and HKM Tanaka. Imaging the density profile of a volcano interior with cosmic-ray muon radiography combined with classical gravimetry. *Measurement Science and Technology*, 23(4):042001, 2012.
- [35] Hiroyuki K.M. Tanaka, Toshiyuki Nakano, Satoru Takahashi, Jyunya Yoshida, Minoru Takeo, Jun Oikawa, Takao Ohminato, Yosuke Aoki, Etsuro Koyama, Hiroshi Tsuji, and Kimio Niwa. High resolution imaging in the inhomogeneous crust with cosmic-ray muon radiography: The density structure below the volcanic crater floor of mt. asama, japan. *Earth and Planetary Science Letters*, 263(1–2):104 – 113, 2007.
- [36] Ryuichi Nishiyama, Akimichi Taketa, Seigo Miyamoto, and Katsuaki Kasahara. Monte carlo simulation for background study of geophysical inspection with cosmic-ray muons. *Geophysical Journal International*, 206(2):1039–1050, 2016.
- [37] H. Asorey, S. Dasso, L.A. Núñez, Y. Pérez, C. Sarmiento-Cano, M. Suárez-Durán, and for the LAGO Collaboration. The LAGO space weather program: Directional geomagnetic effects, background fluence calculations and multi-spectral data analysis. In *The 34th International Cosmic Ray Conference*, volume PoS(ICRC2015), page 142, 2015.
- [38] M. Suárez-Durán. Modulación de rayos cósmicos a nivel del suelo por cambios en el campo geomagnético, para la colaboración lago. Tesis maestría, Escuela de Física, Universidad Industrial de Santander, Bucaramanga, Colombia, 2015.

- [39] L. Desorgher. MAGNETOSCOSMICS, Geant4 application for simulating the propagation of cosmic rays through the Earth magnetosphere. Technical report, Physikalisches Institut, University of Bern, Bern, Germany, 2003.
- [40] J. J. Masías-Meza and S. Dasso. Geomagnetic effects on cosmic ray propagation under different conditions for buenos aires and marambio, argentina. *Sun and Geosphere*, 9:41–47, 2014.
- [41] C. C. Finlay, S. Maus, C. D. Beggan, T. N. Bondar, A. Chambodut, T. A. Chernova, A. Chulliat, V. P. Golovkov, B. Hamilton, M. Hamoudi, R. Holme, G. Hulot, W. Kuang, B. Langlais, V. Lesur, F. J. Lowes, H. Lühr, S. MacMillan, M. Mandea, S. McLean, C. Manoj, M. Menvielle, I. Michaelis, N. Olsen, J. Rauberg, M. Rother, T. J. Sabaka, A. Tangborn, L. Tøffner-Clausen, E. Thébault, A. W. P. Thomson, I. Wardinski, Z. Wei, and T. I. Zvereva. International Geomagnetic Reference Field: the eleventh generation. *Geophysical Journal International*, 183:1216–1230, December 2010.
- [42] N. A. Tsyganenko. A model of the near magnetosphere with a dawn-dusk asymmetry 1. mathematical structure. *Journal of Geophysical Research: Space Physics*, 107(A8):SMP 12–1–SMP 12–15, 2002.
- [43] D. Heck, J. Knapp, J.N. Capdevielle, G. Schatz, and T. Thouw. Corsika : A monte carlo code to simulate extensive air showers. Technical Report FZKA 6019, Forschungszentrum Karlsruhe GmbH, 1998.
- [44] Sergey Ostapchenko. Monte carlo treatment of hadronic interactions in enhanced pomeron scheme: Qgsjet-ii model. *Physical Review D*, 83(1):014018, 2011.
- [45] HC Fesefeldt. Technical report pitha-85-02. Technical Report 5001, III Physikalisches Institut, RWTH Aachen Physikzentrum, 1985.
- [46] S. Agostinelli, J. Allison, K. Amako, J. Apostolakis, H. Araujo, P. Arce, M. Asai, D. Axen, S. Banerjee, G. Barrand, F. Behner, L. Bellagamba, J. Boudreau, L. Broglia, A. Brunengo, H. Burkhardt, S. Chauvie, J. Chuma, R. Chytracek, G. Cooperman, G. Cosmo, P. Degtyarenko, A. Dell'Acqua, G. Depaola, D. Dietrich, R. Enami, A. Feliciello, C. Ferguson, H. Fesefeldt, G. Folger, F. Foppiano, A. Forti, S. Garelli, S. Giani, R. Giannitrapani, D. Gibin, J.J. Gómez Cadenas, I. González, G. Gracia Abril, G. Greeniaus, W. Greiner, V. Grichine, A. Grossheim, S. Guatelli, P. Gumplinger, R. Hamatsu, K. Hashimoto, H. Hasui, A. Heikkinen, A. Howard, V. Ivanchenko, A. Johnson, F.W. Jones, J. Kallenbach, N. Kanaya, M. Kawabata, Y. Kawabata, M. Kawaguti, S. Kelner, P. Kent, A. Kimura, T. Kodama, R. Kokoulin, M. Kossov, H. Kurashige, E. Lamanna, T. Lamp  n, V. Lara, V. Lefebure, F. Lei, M. Liendl, W. Lockman, F. Longo, S. Magni, M. Maire, E. Medernach, K. Minamimoto, P. Mora de Freitas, Y. Morita, K. Murakami, M. Nagamatu, R. Nartallo, P. Nieminen, T. Nishimura, K. Ohtsubo, M. Okamura, S. O'Neale, Y. Oohata, K. Paech, J. Perl, A. Pfeiffer, M.G. Pia, F. Ranjard, A. Rybin, S. Sadilov, E. Di Salvo, G. Santin, T. Sasaki, N. Savvas, Y. Sawada, S. Scherer, S. Sei, V. Sirotenko, D. Smith, N. Starkov, H. Stoecker, J. Sulkimo, M. Takahata, S. Tanaka, E. Tcherniaev, E. Safai Tehrani, M. Tropeano, P. Truscott, H. Uno, L. Urban, P. Urban, M. Verderi, A. Walkden, W. Wander, H. Weber, J.P. Wellisch, T. Wenaus, D.C. Williams, D. Wright, T. Yamada, H. Yoshida, and D. Zschiesche. Geant4: a simulation toolkit. *Nuclear instruments and methods in physics research section A: Accelerators, Spectrometers, Detectors and Associated Equipment*, 506(3):250–303, 2003.

- [47] R. Calderón, H. Asorey, L. A. Núñez, and LAGO Collaboration. Geant4 based simulation of the water cherenkov detectors of the lago project. *Nuclear and Particle Physics Proceedings*, pages 424–426, 2015.
- [48] H. Asorey, R. Calderón-Ardila, L. A. Núñez, J. Peña-Rodríguez, J. Pisco-Guabave, J.D. Sanabria-Gómez, D. Sierra-Porta, M. Suárez-Durán, and A. Vásquez. Mute: design and construction of a muon telescope for the study of the colombian volcanoes. *In preparation*, 2017.
- [49] J. Beringer, J. F. Arguin, R. M. Barnett, K. Copic, O. Dahl, D. E. Groom, C. J. Lin, J. Lys, H. Murayama, C. G. Wohl, W. M. Yao, P. A. Zyla, C. Amsler, M. Antonelli, D. M. Asner, H. Baer, H. R. Band, T. Basaglia, C. W. Bauer, J. J. Beatty, V. I. Belousov, E. Bergren, G. Bernardi, W. Bertl, S. Bethke, H. Bichsel, O. Biebel, E. Blucher, S. Blusk, G. Brooijmans, O. Buchmueller, R. N. Cahn, M. Carena, A. Ceccucci, D. Chakraborty, M. C. Chen, R. S. Chivukula, G. Cowan, G. D'Ambrosio, T. Damour, D. de Florian, A. de Gouvea, T. DeGrand, P. de Jong, G. Dissertori, B. Dobrescu, M. Doser, M. Drees, D. A. Edwards, S. Eidelman, J. Erler, V. V. Ezhela, W. Fettscher, B. D. Fields, B. Foster, T. K. Gaisser, L. Garren, H. J. Gerber, G. Gerbier, T. Gherghetta, S. Golwala, M. Goodman, C. Grab, A. V. Gritsan, J. F. Grivaz, M. Grunewald, A. Gurtu, T. Gutsche, H. E. Haber, K. Hagiwara, C. Hagmann, C. Hanhart, S. Hashimoto, K. G. Hayes, M. Heffner, B. Heltsley, J. J. Hernandez-Rey, K. Hikasa, A. Hoecker, J. Holder, A. Holtkamp, J. Huston, J. D. Jackson, K. F. Johnson, T. Junk, D. Karlen, D. Kirkby, S. R. Klein, E. Klempt, R. V. Kowalewski, F. Krauss, M. Kreps, B. Krusche, Yu V. Kuyanov, Y. Kwon, O. Lahav, J. Laiho, P. Langacker, A. Liddle, Z. Ligeti, T. M. Liss, L. Littenberg, K. S. Lugovsky, S. B. Lugovsky, T. Mannel, A. V. Manohar, W. J. Marciano, A. D. Martin, A. Masoni, J. Matthews, D. Milstead, R. Miquel, K. Moenig, F. Moortgat, K. Nakamura, M. Narain, P. Nason, S. Navas, M. Neubert, P. Nevski, Y. Nir, K. A. Olive, L. Pape, J. Parsons, C. Patrignani, J. A. Peacock, S. T. Petcov, A. Piepke, A. Pomarol, G. Punzi, A. Quadt, S. Raby, G. Raffelt, B. N. Ratcliff, P. Richardson, S. Roesler, S. Rolli, A. Romanouk, L. J. Rosenberg, J. L. Rosner, C. T. Sachrajda, Y. Sakai, G. P. Salam, S. Sarkar, F. Sauli, O. Schneider, K. Scholberg, D. Scott, W. G. Seligman, M. H. Shaevitz, S. R. Sharpe, M. Silari, Torbjörn Sjöstrand, P. Skands, J. G. Smith, G. F. Smoot, S. Spanier, H. Spieler, A. Stahl, T. Stanek, S. L. Stone, T. Sumiyoshi, M. J. Syphers, F. Takahashi, M. Tanabashi, J. Terning, M. Titov, N. P. Tkachenko, N. A. Tornqvist, D. Tovey, G. Valencia, K. van Bibber, G. Venanzoni, M. G. Vincter, P. Vogel, A. Vogt, W. Walkowiak, C. W. Walter, D. R. Ward, T. Watari, G. Weiglein, E. J. Weinberg, L. R. Wiencke, L. Wolfenstein, J. Womersley, C. L. Woody, R. L. Workman, A. Yamamoto, G. P. Zeller, O. V. Zenin, J. Zhang, and R. Y. Zhu. Review of particle physics particle data group. 86(1), 2012.
- [50] T. Uchida, H. K.M. Tanaka, and M. Tanaka. Space saving and power efficient readout system for cosmic-ray muon radiography. *IEEE Transactions on Nuclear Science*, 56(2):448–452, 2009.
- [51] D. Gibert, F. Beauducel, Y. Déclais, N. Lesparre, J. Marteau, F. Nicollin, and A. Tarantola. Muon tomography: Plans for observations in the lesser antilles. *Earth, planets and space*, 62(2):153–165, 2010.
- [52] Ryuichi Nishiyama, Akimichi Taketa, Seigo Miyamoto, and Katsuaki Kasahara. Monte carlo simulation for background study of geophysical inspection with cosmic-ray muons. *Geophysical Journal International*, 206(2):1039–1050, 2016.

- [53] H. Asorey, L.A. Balaguera-Rojas, A .and Núñez, J.D. Sanabria-Gómez, C. Sarmiento-Cano, M. Súarez-Duran, M. Valencia-Otero, and A. Vesga-Ramírez. Astroparticle techniques: Colombia active volcano candidates for muon telescope observation sites. *arXiv preprint arXiv:1704.04967*, 2017.

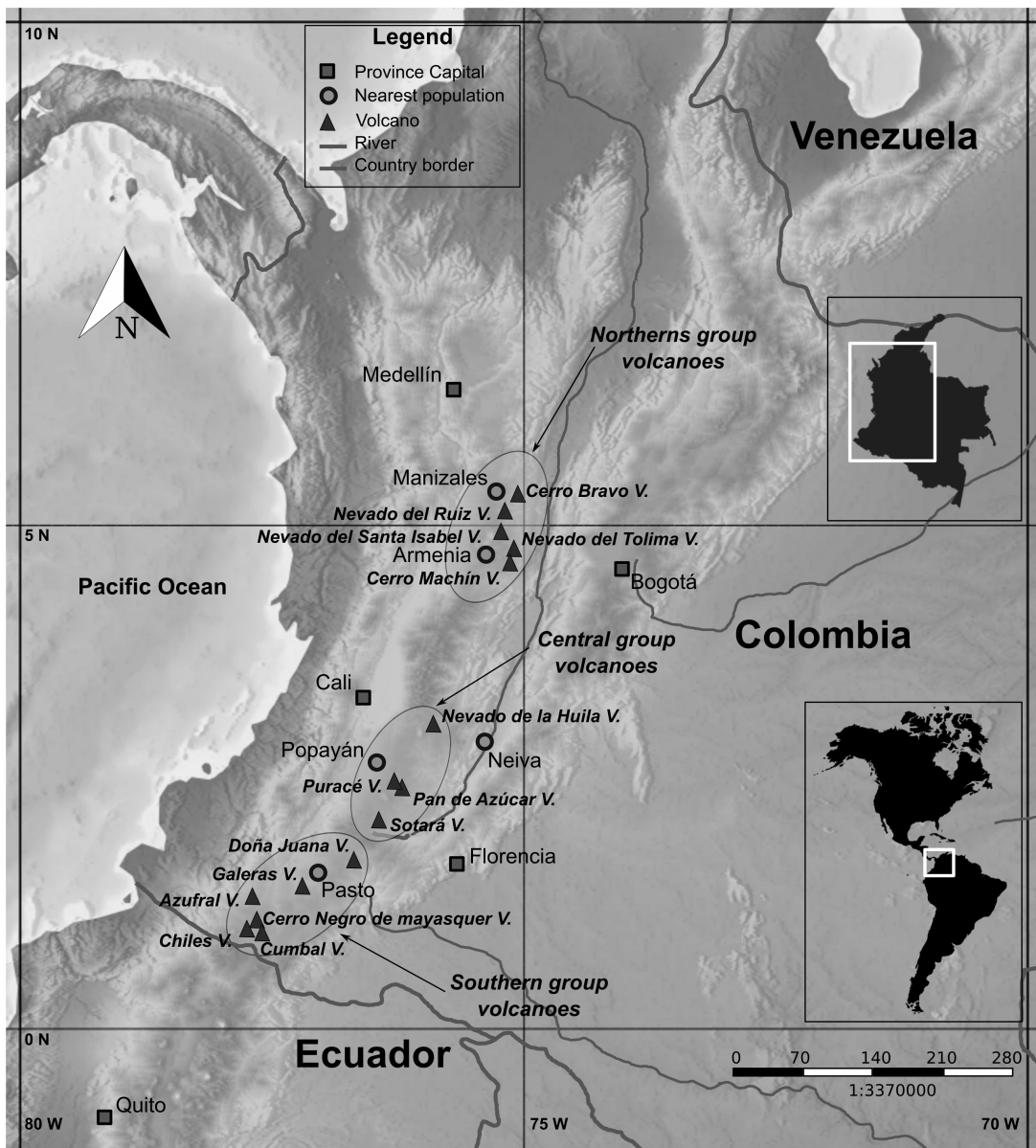


Figure 1: 13 Colombian active volcanoes –Azufral, Cerro Negro, Chiles, Cumbal, Doña Juana, Galeras, Machín, Nevado del Huila, Nevado del Ruiz, Nevado Santa Isabel, Nevado del Tolima, Puracé, and Sotará– are displayed in three disperse clusters through the Cordillera Central. Because of their social significance and eruptive history, we shall briefly focus on four of them: Galeras, Nevado del Ruiz, Cerro Machín and Cerro Negro-Chiles. Galeras, Cerro Negro-Chiles volcanoes are found in the southern cluster, while Nevado del Ruiz and Cerro Machín are located within the most northern one.

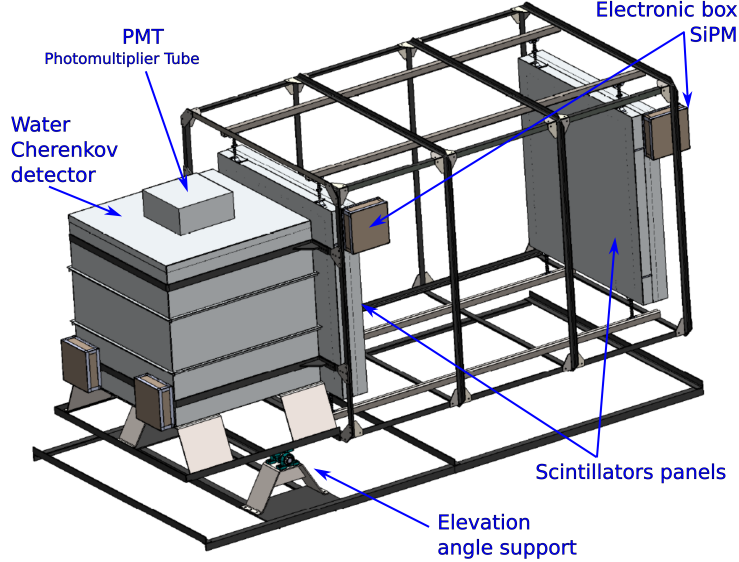


Figure 2: An sketch of our Colombia Muon Telescope (MuTe), which combines the facilities of a two-panel-hodoscope (900 pixels) and 1.73 m^3 water Cherenkov detector. This telescope will be capable to estimate the direction and the range of energies of the detected muons.

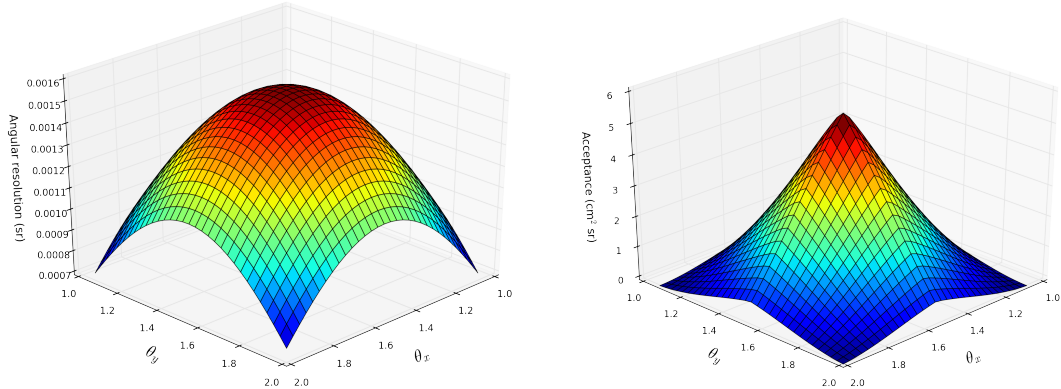


Figure 3: Angular resolution (sr) and acceptance function ($\text{cm}^2 \text{ sr}$) of MuTe. Each detection panel has $N_x = N_y = 30$, 4-cm wide scintillator bars, shaping 900 pixels of 16 cm^2 of detecting area. For a separation of $D = 200 \text{ cm}$ between both panels, there are 3481 discrete r_{mn} possible incoming directions.

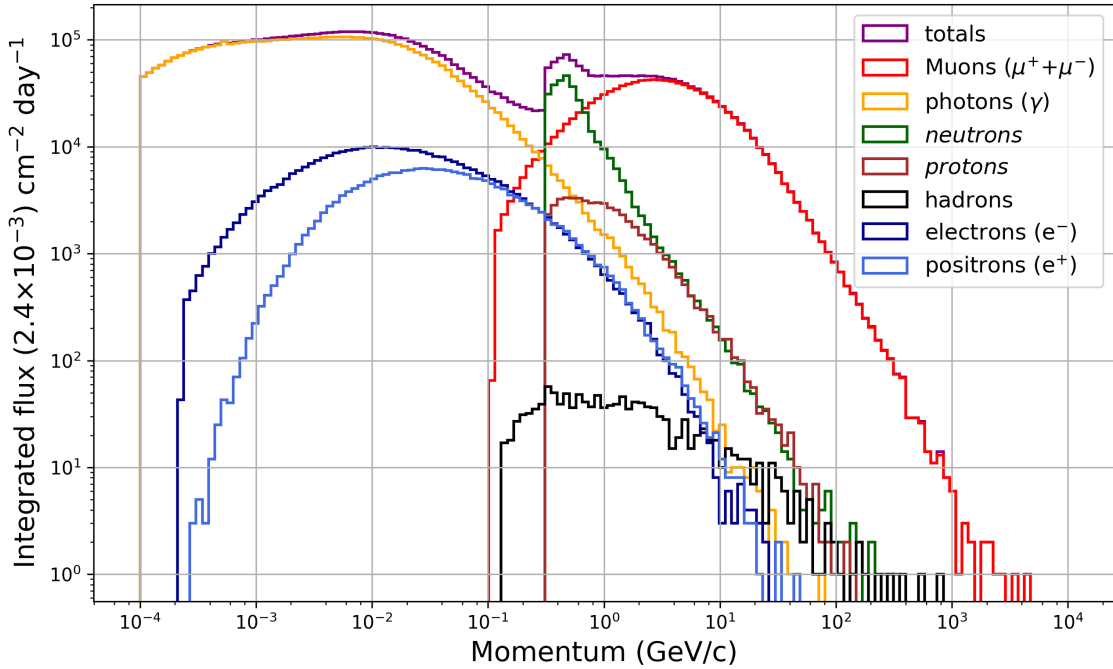


Figure 4: Angular integrated spectrum of secondaries on the selected observation at Cerro Machín. At the highest momentum of the background, the flux is dominated by muons. It is noticeable that muons could reach momenta up to 10 TeV/c but with low occurrence, while the most probable muons arrive on average with an energy of 4 GeV/c.

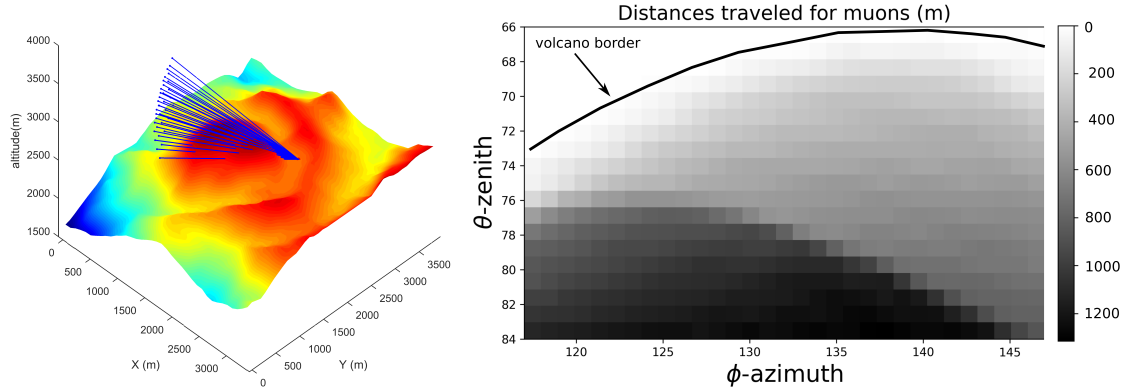


Figure 5: Particle trajectories crossing Cerro Machín volcanic structure to the observation point P_1 , ($4^\circ 29'31''$ N and $75^\circ 22'48''$ W). Notice that for this observation point, muons with zenith angles $\theta > 70^\circ$ travel distances exceeding 900 meters. The topography was obtained from NASA Shuttle Radar Topography Mission global digital elevation model of Earth, with SRTM3 resolution 90m \times 90m.

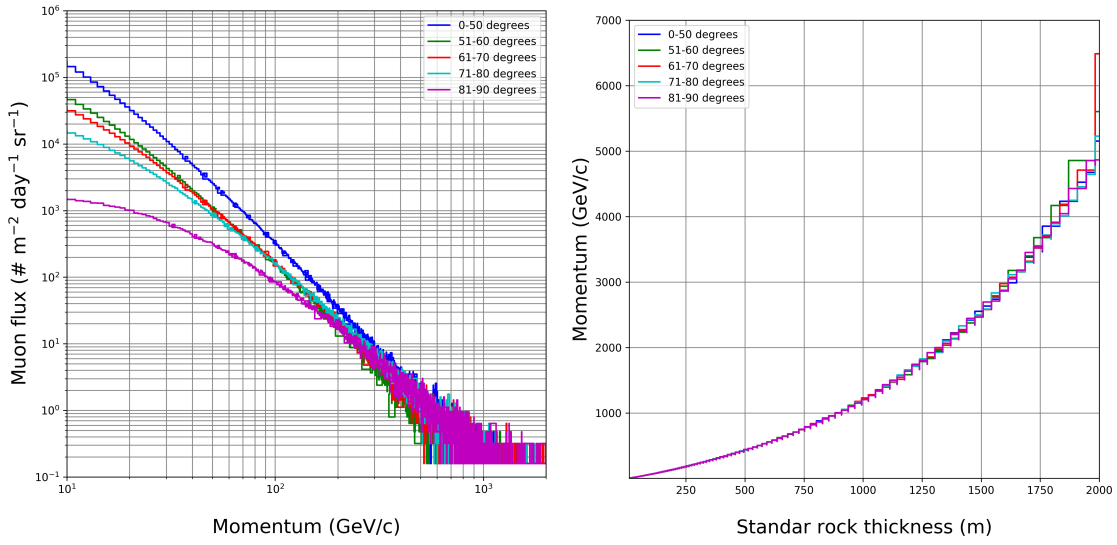


Figure 6: Left plate displays the momentum spectra for muons in five angular bins after crossing a variable standard rock with density 2.65 g/cm^3 . At $p_\mu \simeq 500 \text{ GeV}/c$, the expected integrated flux is $1 \text{ cm}^{-2} \text{ sr}^{-1} \text{ day}^{-1}$. As is expected, muons with zenith angles close to the horizontal decrease by a factor of 100 with respect to muons with angles of incidence more vertical. Right plate illustrates the muon energy needed to cross standard rock (2.65 g/cm^3) thickness.

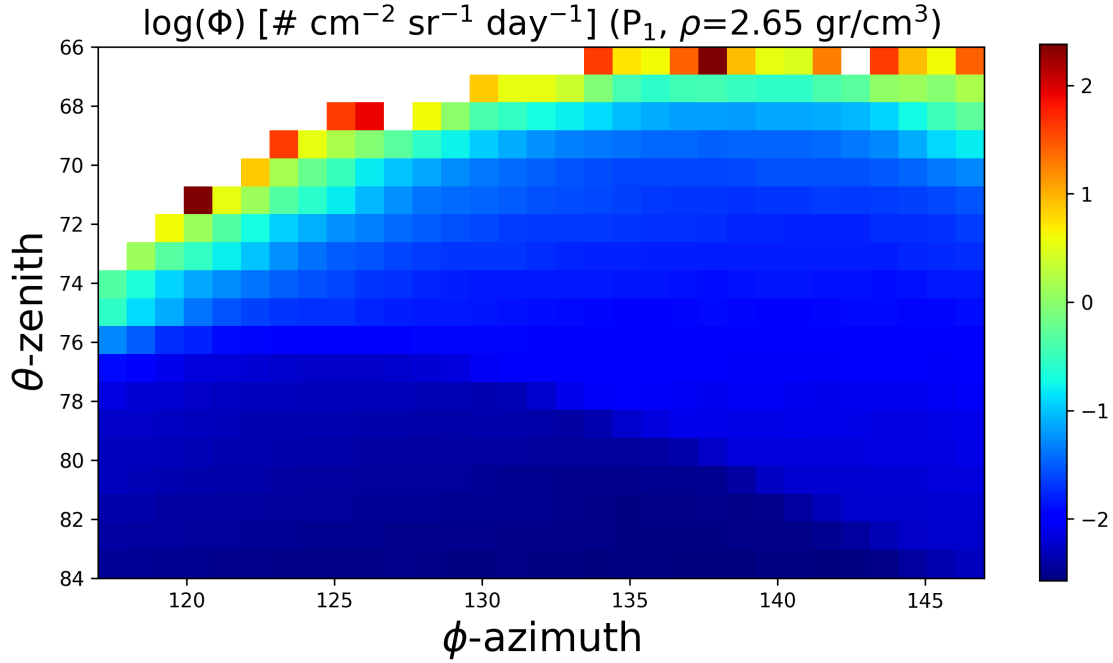


Figure 7: Expected muon flux at observation point \mathbf{P}_1 in Cerro Machín, as a function of the direction of incidence, for azimuthal range $116 < \phi < 147$ and zenithal range $66 < \theta < 84$. Muons with energies from 0.1 GeV/c to 10 TeV, generate feeble flux: $\approx 10^{-2}$ muon per square centimeter per day at the maximum possible observed depth at zenith angles $\theta \approx 82 - 84$. White pixels represent open sky muon flux, other colors illustrate the emerging muon flux from the volcano edifice.

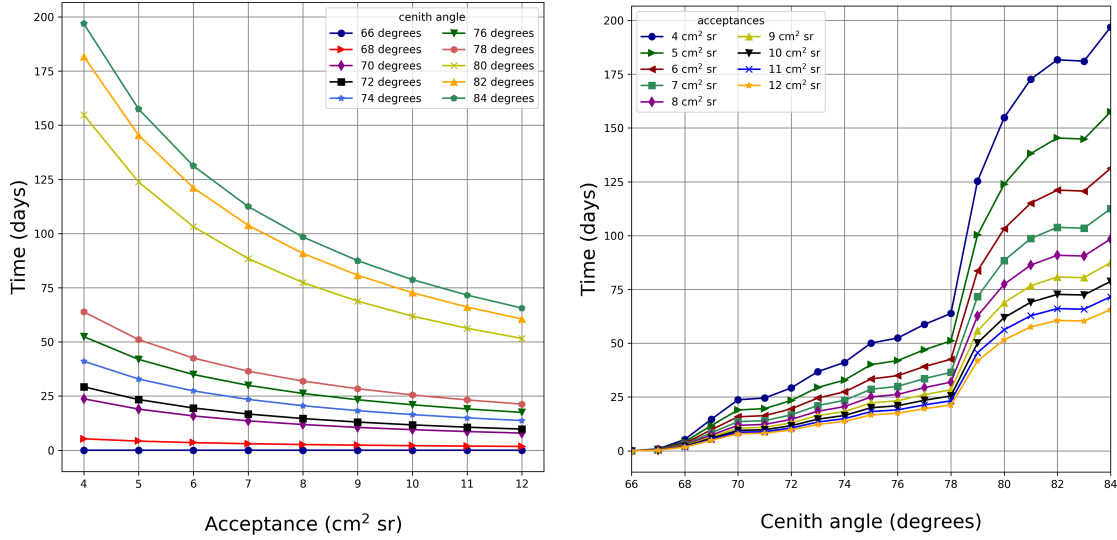


Figure 8: Exposure times for observation point \mathbf{P}_1 at Cerro Machín needed to identify differences of -10% in the averaged directional density for different zenith angles and telescope acceptance. We obtain exposure time lapses between two days up to more than six months to obtain the desired density resolution, at different zenith angles.